A Journal of the Gesellschaft Deutscher Chemiker

Angewandte International Edition Chemie

GDCh

www.angewandte.org

Accepted Article

Title: Biomimetic chiral photonic crystals

Authors: Jiawei Lv, Defang Ding, Xuekang Yang, Ke Hou, Xiang Miao, Dawei Wang, Baichuan Kou, Ling Huang, and Zhiyong Tang

To be cited as: *Angew. Chem. Int. Ed.* 10.1002/anie.201903264
Angew. Chem. 10.1002/ange.201903264

Link to VoR: http://dx.doi.org/10.1002/anie.201903264
http://dx.doi.org/10.1002/ange.201903264

WILEY-VCH

10.1002/anie.201903264

WILEY-VCH

Biomimetic chiral photonic crystals

Jiawei Lv[a,b], Defang Ding[c], Xuekang Yang[a], Ke Hou[a], Xiang Miao[a], Dawei Wang[a], Baichuan Kou[a], Ling Huang[b], Zhiyong Tang*[a]

Abstract: Although it is well known that the amazing iridescent colors from the cuticle of beetles reflect intricate nanoscale organization of bio-fibers, artificial inorganic materials with comparable optical response have not yet been synthesized with abiotic nano-building blocks. Such materials have broad applications including circular polarizers, circularly polarized luminescence, lasers, etc. Here, we describe a general method to fabricate biomimetic chiral photonic crystals via Langmuir-Schaefer assembly of colloidal inorganic nanowires. We not only reproduce the intricate helical structure and circularly polarized color reflection in beetles, but also acquire the highest chiroptical activity with a dissymmetry factor of -1.6 among the chiral inorganic nanostructures. More importantly, beyond nature, programmable structural control based on the precise interlayer arrangement endows us an unprecedented freedom to manipulate the optical activity of as-fabricated chiral photonic crystals.

Colors are essential for the survival of animals and plants in nature[1]. Specifically, the structural colors, which result from the scattering, interference and diffraction of light with periodic dielectric materials having a feature size comparable to the visible light wavelength, are prevalent in the biological world[2]. Among the various structural colors developed in nature, one amazing category is circular dichroism[3]. The cuticles of many scarabaeid beetles are able to selectively reflect left circularly polarized light, thus showing distinct optical appearances (Figure 1a and Figure S1) viewed through left and right circular polarizers[3b, 3c]. Detailed investigations reveal the layered structures inside the cuticles (Figure 1b). In each layer parallel with the surface plane, chitin nanofibers[4] are aligned in the same direction, while the adjacent layer rotates its alignment direction clockwise with a small angle (Figure 1c). The continuous rotation of the alignment direction creates the periodical helical superstructures with a pitch length comparable to the wavelength of visible light, leading to formation of vertical one-dimensional photonic crystals with strong Bragg reflection. For incidence normal to the surface plane, the wavelength of the first-order Bragg reflection peak (λ_0) is determined by $\lambda_0 = nP$ (Eq. 1), where n is the average refraction index and P is helical pitch length. The P corresponds to the vertical distance required when the alignment direction of the building layers rotates 360° (Fig. 1c). Besides, the width of the reflection peak ($\Delta\lambda$) is associated with the birefringence ($\Delta n = n_e - n_o$) in the building layers, namely $\Delta\lambda = P\Delta n$ (Eq. 2), where n_e and n_o are the refractive index for light polarized parallel and orthogonal to the alignment direction, respectively. Such structure feature is also found in plants like the shiny fruit of Pollia Condensata[3d].

Encouraged by the unique optical activity of natural chiral photonic crystals, the artificial analogies have been prepared by either bottom-up or top-down methods. Typically, bottom-up methods rely on self-assembly of bio-derived materials, such as cellulose nanocrystals[5]. A big advantage is biological abundance of the building blocks. However, due to the homochirality in nature, only left handed chiral photonic crystals are achieved from these materials[5d]. On the contrary, top-down methods can afford rich structure design through a variety of fabrication techniques[6]. Unfortunately, these methods usually require very expensive equipment, and more seriously the chiral photonic crystals with optical response in the UV-visible range are difficult to be acquired owing to the limited resolution of current three-dimensional fabrication[7].

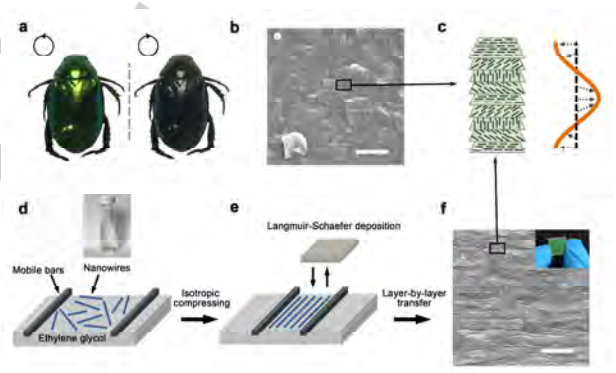

Figure 1. A biomimetic route to chiral photonic crystals. (a) Photos of Anomala corpulenta Motschulsky (one type of scarabaeid beetle) taken through left (left photo) or right (right photo) circular polarizer, respectively. (b) Scanning electron microscope (SEM) image of cross section of cuticle of Anomala corpulenta Motschulsky, showing layered structure. (c) Scheme of helical arrangement of aligned layers to constitute chiral photonic crystals. (d) Dispersing nanowires at air-liquid interface in Langmuir trough, and the top is photo of cyclohexane solution containing $NiMoO_4 \cdot xH_2O$ nanowires. (e) Compressing barriers to obtain aligned nanowire films, followed by transferring the aligned layer onto a substrate via horizontal lifting (Langmuir-Schaefer deposition). (f) SEM image of cross section of chiral photonic crystal film through layer-by-layer transfer with a predesigned twisting angle, and inset is the corresponding photo of film. Scale bars are 2 μm for (b) and (f).

In this work, we propose fabricating biomimetic chiral photonic crystals through layer-by-layer Langmuir-Schaefer assembly[8]. As-synthesized nanowires (Figure S2) floating on the surface of subphase in a Langmuir trough are slowly compressed with two mobile bars to achieve a nanowire film with uniaxial alignment (Figure 1d,e). Afterwards, the aligned nanowire film is transferred to a quartz plate by Langmuir-Schaefer method to form the first layer. Before transferring next nanowire film layer, the quartz plate is rotated horizontally with a specified angle clockwise or anti-clockwise to obtain left or right handed photonic crystals, respectively (Figure 1f). When the rotation angle (α) is varied, the number of layers (L) needed for a full pitch is also altered ($L = 360°/\alpha$). Since the pitch length $P = L * T$, where T is the thickness of each film layer, the optical activity of chiral photonic crystals is thereof tuned. Noteworthily, the bottom-up Langmuir-Schaefer assembly easily produces large-area highly aligned nanowire films, while the top-down

[a] Dr. J. Lv, K. Hou, X. Yang, X. Miao, Dr. D. Wang, B. Kou, Prof. Z. Tang.
CAS Key Laboratory for Nanosystem and Hierarchy Fabrication,
CAS Center for Excellence in Nanoscience
National Center for Nanoscience and Technology,
Beijing 100190, P.R. China
E-mail: zytang@nanoctr.cn
[b] Dr. J. Lv, Prof. L. Huang
Key Laboratory of Flexible Electronics (KLOFE) & Institute of Advanced Materials (IAM), Jiangsu National Synergetic Innovation Center for Advanced Materials (SICAM)
Nanjing Tech University, (NJTECH)
30 South Puzhu Road , Nanjing 211816, P.R. China
[c] Dr. D. Ding
Faculty of Materials Science and Chemistry
China University of Geosciences
Wuhan 430074, P. R. China

layer-by-layer transfer allows precise control over both rotation direction and angle. As a result, diversified chiral photonic crystals are expected to be acquired.

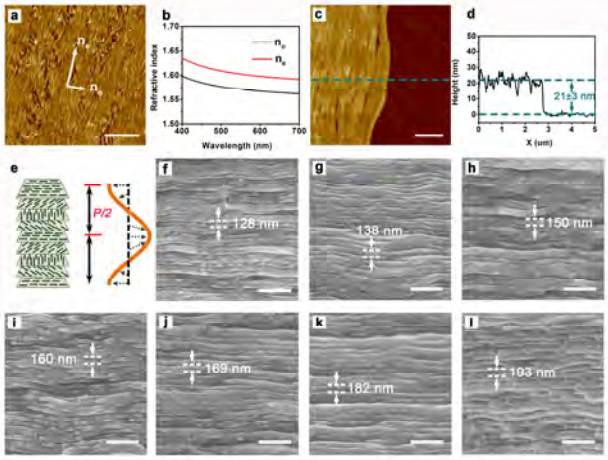

Figure 2. Structures of biomimetic chiral photonic crystals**.** (a) AFM image of aligned nanowires in one film layer. (b) Refractive index of ordinary ray (n_o) and extraordinary ray (n_e) shown in (a). (c, d**)** AFM measurement of thickness of one nanowire film layer. (e**)** Scheme denoting half pitch of chiral structure. (f) to (l), SEM sectional images of chiral photonic crystals. From (f) to (l), each pitch contains 11 to 17 nanowire film layers. Scale bars are 5 μm for (a), 1 μm for (c), and 500 nm for (f) to (l).

Ultrathin $NiMoO_4 \cdot xH_2O$ nanowires of diameters less than 2 nm are selected as the building blocks[9] because of twofold reasons (Figure S2): they possess negligible optical absorption in the visible range, and the ultrathin nature leaves large freedom to adjust the *P*. Atomic force microscope (AFM) imaging confirms large-area alignment of nanowires in the film layer (Figure 2a), causing the notable birefringence[10] across the visible range (Figure 2b). Note that the film layer has uniform *T* of ~21 nm (Figure 2c,d). As typical examples, seven right handed photonic crystals with different *P* are constructed by varying *L* from 11 to 17 via anticlockwise transfer, and each sample contains total 1,000 film layers to exclude possible optical influence from different amounts of nanowires (Figure S3). The cross-sectional SEM images show the clear periodic structure typical of chiral photonic crystals (Figure 2f-l). It needs to be noticed that the periodic distance observed in SEM images corresponds to one half pitch length (*P/2* in Figure 2e), which comprises multiple nanowire film layers. As expected, the periodic distance grows with the increasing *L* (Figure 2f-l), and an incremental value is approximately half *T* of a nanowire film layer (Figure 2d).

Impressively, analogous to their bio-counterparts[3b, 3d], as-fabricated chiral photonic crystals exhibit vivid colors ranging from violet to red (Figure 3a). With right handed structures, the samples selectively reflect right circularly polarized light without changing the handedness of light[11]. As a result, one can observe the reflected colors through a right circular polarizer (Figure 3a). In sharp contrary, these seven samples appear in the same gray color under a left circular polarizer because the reflected right circularly polarized light is blocked (Figure 3b).

Circular dichroism (CD) spectroscopy is adopted to accurately characterize the optical activity of chiral photonic crystals, and several prominent characteristics are distinguished. First, all the seven samples show very strong negative CD peaks at the wavelength positions in accordance to their optical appearances (Figure 3c). Notably, these CD peaks are very sharp with full width at half maximum (FWHM) generally smaller than 30 nm (Figure S4), comparable to the best-quality absorption or photoluminescence peaks of nanostructures[12]. Similarly, both absorption and reflection spectra also display the distinct peaks originating from Bragg reflection (bottom curves in Figure 3c and Figure 3d). Second, the CD peak position gradually red shifts with increasing *L* (Figure 3c). It deserves to be stressed that the average refraction index *n* deduced by peak position and pitch length (Eq. 1) is very close to the measured value (Figure S5), validating the structure-optical activity model of chiral photonic crystals. Third, the *g*-factor, a dimensionless factor that quantifies the chiroptical strength of chiral materials, reaches -1.6 in samples *A13* to *A17* (Figure 3e), approaching the theoretical limit of ±2[13]. As for samples *A11* and *A12*, the *g*-factor is relatively smaller because there is considerable intrinsic absorption of $NiMoO_4 \cdot xH_2O$ nanowires in the wavelength region shorter than 450 nm (Figure 3c and S2). Nevertheless, the *g*-factor of all the samples is larger than -1. Such giant value is essential for practical application like circular polarizers[6, 14], circular polarized luminescence[5b, 15], lasers[16], etc. Fourth, the left handed chiral photonic crystals with mirror-symmetric CD responses are easily acquired by reversing the transfer manner (Figure S6). The CD intensity grows as the pitch number increases, which well matches with the theoretical model (Figure S7)[17]. Fifth, additional strong CD response is discerned in the UV range shorter than 400 nm (Figure S8), attributing to the birefringence and linear dichroism of the aligned nanowires[8a]. Sixth, the prepared chiral photonic crystals exhibit excellent stability under ambient condition (Figure S9), thanks to high chemical and physical robustness of inorganic nanowires. Last but not the least, the method for fabrication of chiral photonic crystals is universal. For instance, when ultrathin GdOOH[18] nanowires are used as the alternative building blocks, the tunable CD responses in the UV range of 200-300 nm are obtained (Figure S10), due to very thin thickness of each film layer (~8 nm).

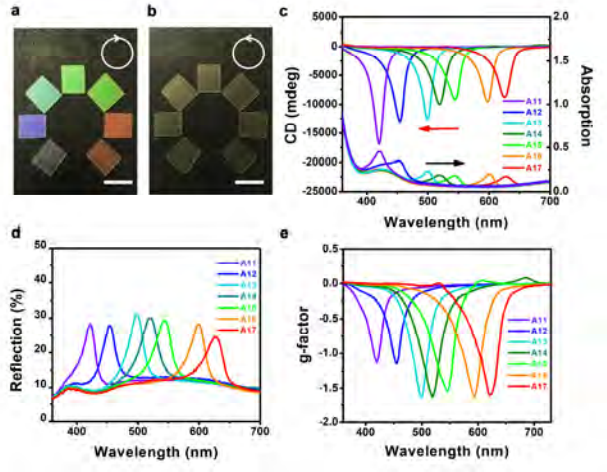

Figure 3. Optical characterizations. Chiral photonic crystals viewed through right (a) or left (b) circular polarizer. (c) CD and absorption spectra of seven samples. A11 - A17 stand for samples with a full pitch containing anticlockwise rotated 11 - 17 nanowire film layers, respectively. (d) Reflection spectra of samples. (e) The *g*-factor of the samples. Scale bars are 1 cm for (a) and (b).

Armed with arbitrary control over the CD response with respect to peak sign, position and intensity, we demonstrate an

optical security system based on CD spectra (Figure 4a). For spectroscopy coding, the coding capacity scales with X^Y[19], where ***X*** and ***Y*** refer to the number of peak position and intensity, respectively. Evidently, compared with current spectroscopy coding techniques[20], CD spectroscopy coding has many unique advantages including positive and negative peak signs, tunable

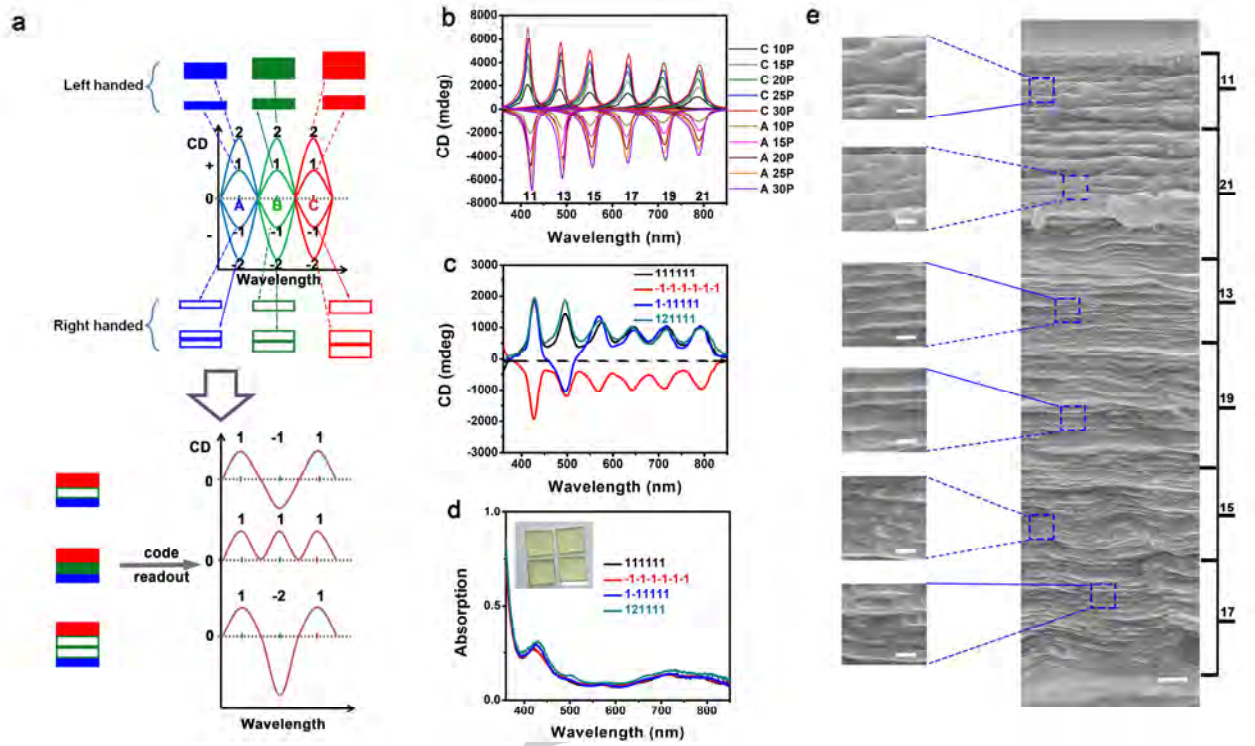

Figure 4. Demonstration of CD spectroscopy coding. (a) Scheme of coding and readout process. A calibration curve is firstly established to correlate the structure, CD peak and digital information (top panel). Herein, each rectangle represents a certain number of pitches. Afterwards, the codes are built with combination of the building elements and then readout as digital information by comparing with the calibration curve (bottom panel). (b) CD intensity variation with pitch number at 6 different peak positions. The number above the horizontal axis represents the number of film layers to implement a full pitch, determining the pitch length. As for right labels, C 10P stands for the sample containing 10 pitches formed with clockwise transfer, while A 10P denotes the sample formed with anticlockwise transfer. (c) CD spectra of 4 coding samples. Each sample is readout as the digital sequence shown in the corresponding label. (d) Absorption spectra corresponding to (c). Inset is the photo of four samples taken under natural light. (e) SEM cross-sectional image of a coded sample named 111111. The number highlights that the sample contains six regions with CD response at different wavelengths. Scale bars are 1 cm for (d), 200 nm for the left images in (e), and 1 μm for the right image.

peak positions from violet to red, narrow FWHM peaks, and free interference between different peaks (Figure S11). Therefore, one might code a sample with multiple CD peaks but minimal overlap over a large wavelength range, which assures large coding capacity. In a typical coding process, a standard CD spectrum is firstly established, in which the peak position and intensity are directly associated with the pitch length and number of chiral photonic crystals. Using 3 peak positions (A, B and C) and 4 peak intensities (-2, -1, 1 and 2) as illustration (top panel in Figure 4a), the digital points are coded by selective integration of A to C and -2 to 2 in a chiral photonic crystal, followed by readout with reference of the standard spectrum (bottom panel in Figure 4a).

In the experiments, we bring about 6 peak positions and 10 peak intensities, thus affording a coding capacity of 10^6 (Figure 4b-d). At each peak position, five positive intensities are correlated to number 1 to 5 with increasing magnitude, while the negative intensities with increasing absolute value are assigned to number -1 to -5. It is noticed that in the real standard spectrum (Figure 4b), the CD intensity gradually decreases as the wavelength increases, mainly owing to the decreasing birefringence in the film layers (Figure S12). Figure 4c exemplifies four coding samples, and each code is conveniently and clearly readout according to the standard spectrum. Significantly, these four samples show very similar optical appearances (inset in Figure 4d) and absorption spectra (Figure 4d), which are hardly distinguished by naked eye or conventional spectroscopy. The cross sectional SEM imaging on the 111111 sample in Figure 4c further clarifies the coding mechanism (Figure 4e). One can see that the encoded film is composed of six parts with different pitch lengths as designed, corresponding to six peaks in the coded CD spectra.

In summary, biomimetic chiral photonic crystals are successfully constructed and exhibit extremely large chiroptical responses. Remarkably, these chiroptical responses can be arbitrarily tuned with programmed structural design, giving rise to CD spectroscopy coding with high capacity and fidelity. We believe the optical security capacity is expected to be furtherly increased in combination with graphical coding[21]. Our method is universal and robust. We envision that many inorganic nanomaterials with excellent optical, electrical and magnetic properties are readily incorporated into the chiral photonic crystals to afford emerging multifunctional devices.

Acknowledgements

The authors acknowledge financial support from National Key Basic Research Program of China (2014CB931801 and 2016YFA0200700, Z.Y.T.), National Natural Science Foundation of China (21721002 and 21475029, Z.Y.T.), Frontier Science Key Project of Chinese Academy of Sciences (QYZDJ-SSW-SLH038, Z.Y.T.), "Strategic Priority Research Program" of Chinese Academy of Sciences (XDA09040100, Z.Y.T.), and K.C.Wong Education Foundation (Z.Y.T.).

Keywords: Biomimetics • self-assembly • Langmuir-Blodgett films • chirality • nanowires

[1] A. G. Dumanli, T. Savin, *Chem. Soc. Rev.* **2016**, *45*, 6698-6724.

[2] a) S. Tadepalli, J. M. Slocik, M. K. Gupta, R. R. Naik, S. Singamaneni, *Chem. Rev.* **2017**, *117*, 12705-12763; b) A. R. Parker, H. E. Townley, *Nat. Nanotechnol.* **2007**, *2*, 347-353; c) T. B. H. Schroeder, J. Houghtaling, B. D. Wilts, M. Mayer, *Adv. Mater.* **2018**, *30*, 1705322.

[3] a) A. C. Neville, S. Caveney, *Biol. Rev*. **1969**, *44*, 531-562; b) V. Sharma, M. Crne, J. O. Park, M. Srinivasarao, *Science* **2009**, *325*, 449-451; c) L. F. del Rio, H. Arwin, K. Jarrendahl, *Thin Solid Films* **2014**, *571*, 410-415; d) S. Vignolini, P. J. Rudall, A. V. Rowland, A. Reed, E. Moyroud, R. B. Faden, J. J. Baumberg, B. J. Glover, U. Steiner, *Proc. Natl. Acad. Sci. U.S.A.* **2012**, *109*, 15712-15715.

[4] S. Ling, D. L. Kaplan, M. J. Buehler, *Nat. Rev. Mater.* **2018**, *3*, 18016.

[5] a) K. E. Shopsowitz, H. Qi, W. Y. Hamad, M. J. MacLachlan, *Nature* **2010**, *468*, 422-425; b) H. Z. Zheng, W. R. Li, W. Li, X. J. Wang, Z. Y. Tang, S. X. A. Zhang, Y. Xu, *Adv. Mater.* **2018**, *30*, 1705948; c) R. M. Parker, G. Guidetti, C. A. Williams, T. Zhao, A. Narkevicius, S. Vignolini, B. Frka-Petesic, *Adv. Mater.* **2018**, *30*, 1704477; d) A. P. C. Almeida, J. P. Canejo, S. N. Fernandes, C. Echeverria, P. L. Almeida, M. H. Godinho, *Adv. Mater.* **2018**, *30*, 1703655.

[6] a) J. K. Gansel, M. Thiel, M. S. Rill, M. Decker, K. Bade, V. Saile, G. von Freymann, S. Linden, M. Wegener, *Science* **2009**, *325*, 1513-1515; bY. Zhao, M. A. Belkin, A. Alu, *Nat. Commun.* **2012**, *3*, 7.

[7] M. Thiel, G. von Freymann, M. Wegener, *Opt. Lett.* **2007**, *32*, 2547-2549.

[8] a) J. W. Lv, K. Hou, D. F. Ding, D. W. Wang, B. Han, X. Q. Gao, M. Zhao, L. Shi, J. Guo, Y. L. Zheng, X. Zhang, C. G. Lu, L. Huang, W. Huang, Z. Y. Tang, *Angew. Chem*. **2017**, *129*, 5137–5142; *Angew. Chem. Int. Ed.* **2017**, *56*, 5055-5060; b) F. Kim, S. Kwan, J. Akana, P. D. Yang, *J. Am. Chem. Soc.* **2001**, *123*, 4360-4361; c) A. Tao, F. Kim, C. Hess, J. Goldberger, R. R. He, Y. G. Sun, Y. N. Xia, P. D. Yang, *Nano Lett.* **2003**, *3*, 1229-1233; d) P. Yang, *Nature* **2003**, *425*, 243-244; e) D. Whang, S. Jin, Y. Wu, C. M. Lieber, *Nano Lett.* **2003**, *3*, 1255-1259; f) J. W. Liu, J. H. Zhu, C. L. Zhang, H. W. Liang, S. H. Yu, *J. Am. Chem. Soc.* **2010**, *132*, 8945-8952.

[9] H. L. Liu, H. Y. Li, P. L. He, X. Wang, *Small* **2016**, *12*, 1006-1012.

[10] O. L. Muskens, M. T. Borgström, E. P. A. M. Bakkers, J. Gómez Rivas, *Appl.Phys. Lett.* **2006**, *89*, 233117.

[11] H. Devries, *Acta Crystallogr.* **1951**, *4*, 219-226.

[12] a) G. Gonzalez-Rubio, P. Diaz-Nunez, A. Rivera, A. Prada, G. Tardajos, J. Gonzalez-Izquierdo, L. Banares, P. Llombart, L. G. Macdowell, M. A. Palafox, L. M. Liz-Marzan, O. Pena-Rodriguez, A. Guerrero-Martinez, *Science* **2017**, *358*, 640-644; b) J. H. Zhou, M. Y. Zhu, R. Y. Meng, H. Y. Qin, X. G. Peng, *J. Am. Chem. Soc.* **2017**, *139*, 16556-16567.

[13] a) H.-E. Lee, H.-Y. Ahn, J. Mun, Y. Y. Lee, M. Kim, N. H. Cho, K. Chang, W. S. Kim, J. Rho, K. T. Nam, *Nature* **2018**, *556*, 360-365. b) M. Z. Sun, L. G. Xu, A. H. Qu, P. Zhao, T. T. Hao, W. Ma, C. L. Hao, X. D. Wen, F. M. Colombari, A. F. de Moura, N. A. Kotov, C. L. Xu, H. Kuang, *Nat. Chem.* **2018**, *10*, 821-830; c) W. J. Yan, L. G. Xu, C. L. Xu, W. Ma, H. Kuang, L. B. Wang, N. A. Kotov, *J. Am. Chem. Soc.* **2012**, *134*, 15114-15121; d) W. Ma, P. Fu, M. Z. Sun, L. G. Xu, H. Kuang, C. L. Xu, *J. Am. Chem. Soc.* **2017**, *139*, 11752-11759; e) X. Zhao, L. Xu, M. Sun, W. Ma, X. Wu, C. Xu, H. Kuang, N*at. Commun.* **2017**, *8*, 2007. f) W. Ma, L. G. Xu, A. F. de Moura, X. L. Wu, H. Kuang, C. L. Xu, N. A. Kotov, *Chem. Rev.* **2017**, *117*, 8041-8093.

[14] D. J. Broer, J. Lub, G. N. Mol, *Nature* **1995**, *378*, 467-469.

[15] S. H. Chen, D. Katsis, A. W. Schmid, J. C. Mastrangelo, T. Tsutsui, T. N. Blanton, *Nature* **1999**, *397*, 506-508.

[16] H. Coles, S. Morris, *Nat. Photon.* **2010**, *4*, 676-685.

[17] S. Chandrasekhar, J. S. Prasad, *Mol. Cryst. Liq. Cryst.* **1971**, *14*, 115-128.

[18] S. Hu, H. L. Liu, P. P. Wang, X. Wang, *J. Am. Chem. Soc.* **2013**, *135*, 11115-11124.

[19] M. Y. Han, X. H. Gao, J. Z. Su, S. Nie, *Nat. Biotechnol.* **2001**, *19*, 631-635.

[20] S. Shikha, T. Salafi, J. T. Cheng, Y. Zhang, *Chem.Soc. Rev.* **2017**, *46*, 7054-7093.

[21] H. Lee, J. Kim, H. Kim, J. Kim, S. Kwon, *Nat. Mater.* **2010**, *9*, 745-749.

10.1002/anie.201903264

WILEY-VCH

COMMUNICATION

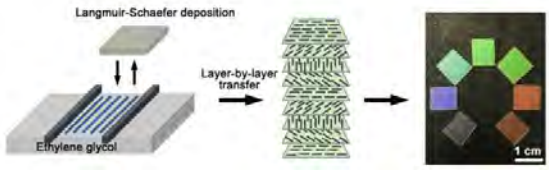

A biomimetic route to fabricating chiral photonic crystals via layer-by-layer Langmuir-Schaefer assembly is demonstrated. This method offers precise control over the structures and optical activities, showing potential application in CD spectroscopy coding.

*Jiawei Lv, Defang Ding, Xuekang Yang, Ke Hou, Xiang Miao, Dawei Wang, Baichuan Kou, Ling Huang, Zhiyong Tang**

Page No. – Page No.

Biomimetic chiral photonic crystals